Journal of Geophysical Research: Planets

RESEARCH ARTICLE
10.1029/2018JE005561

Special Section:
Science and Exploration of the Moon, Near-Earth Asteroids, and the Moons of Mars

Can Formulas Derived From Pyroxenes and/or HEDs Be Used to Determine the Mineralogies of V-Type Asteroids?

T. H. Burbine[1], P. C. Buchanan[2], R. L. Klima[3], and R. P. Binzel[4]

[1]Department of Astronomy, Mount Holyoke College, South Hadley, MA, USA, [2]Department of Chemistry, Kilgore College, Kilgore, TX, USA, [3]Applied Physics Laboratory, The Johns Hopkins University, Laurel, MD, USA, [4]Department of Earth, Atmospheric, and Planetary Sciences, Massachusetts Institute of Technology, Cambridge, MA, USA

Key Points:
- Formulas derived from basaltic achondrite spectra with measured compositions can be used to determine the pyroxene mineralogies of V-type asteroids
- Most of these observed V-type near-Earth asteroids have interpreted mineralogies similar to eucrites or howardites

Correspondence to:
T. H. Burbine,
tburbine@mtholyoke.edu

Citation:
Burbine, T. H., Buchanan, P. C., Klima, R. L., & Binzel, R. P. (2018). Can formulas derived from pyroxenes and/or HEDs be used to determine the mineralogies of V-type asteroids? *Journal of Geophysical Research: Planets*, *123*. https://doi.org/10.1029/2018JE005561

Received 29 JAN 2018
Accepted 7 JUN 2018
Accepted article online 19 JUN 2018

Abstract We compare methods for determining the pyroxene mineralogies of V-type near-Earth asteroids from their reflectance spectra. We evaluate whether band centers derived from the spectra of synthetic pyroxenes can be used to achieve greater analytical accuracy than is achieved through the use of band centers derived from the spectra of basaltic achondrites (howardites, eucrites, diogenites or HEDs). We conclude that band centers derived from the reflectance spectra of synthetic pyroxenes with known mineralogies do not provide useful diagnostic information to derive equations for determining accurate pyroxene compositions of V-type asteroids. Band centers from the reflectance spectra of HEDs with known pyroxene mineralogies can be used to derive equations for determining accurate pyroxene compositions of V-type asteroids. HEDs are physical mixtures of a number of different types of pyroxenes and best simulate the surfaces of V-type asteroids. Formulas using the Band I center appear best for determining asteroid pyroxene mineralogies for V-type asteroids due to the current difficulty in doing accurate temperature corrections to the Band II center. Most of the observed V-type near-Earth asteroids have interpreted mineralogies similar to eucrites or howardites. One of the observed near-Earth asteroids could possibly have a surface mineralogy similar to diogenites.

Plain Language Summary We have tested whether relatively simple formulas can be derived to determine the mineralogies of pyroxene-rich asteroids with interpreted mineralogies similar to basaltic achondrites and their proposed parent body (4) Vesta. We have concluded that the best way to derive formulas for determining the mineralogies of asteroids is to use meteorites with mineralogies that appear similar to asteroids and not homogeneous pyroxenes since meteorites best simulate the characteristics of asteroid surfaces. We have determined the pyroxene mineralogies for a number of V-type near-Earth asteroids. We have found that most of the observed V-type near-Earth asteroids have mineralogies similar to eucrites or diogenites.

1. Introduction

Many methods have been used to estimate asteroid mineralogies. These methods include curve matching (e.g., Chapman & Salisbury, 1973), absorption band modeling (e.g., Sunshine et al., 2007), radiative transfer modeling (e.g., Lawrence & Lucey, 2007), and formulas using derived spectral parameters (e.g., Dunn et al., 2010; Gaffey et al., 2002). The goals of these methods are to determine the abundances of different minerals on the asteroids' surfaces and/or the composition of their minerals.

FeO-bearing pyroxenes tend to have a symmetric Band I centered near ~1 μm and a symmetric Band II centered near ~2 μm (Figure 1) due to the absorption of photons by electrons in the *3d* orbitals of Fe^{2+}. The exceptions are high-Ca pyroxenes (Schade et al., 2004), which can have a broad Band I and a weak to absent Band II. The band center positions for pyroxenes are known to be a function of their mineralogy (e.g., Cloutis & Gaffey, 1991). Pyroxene band centers tend to move to longer wavelengths with increasing contents of iron and/or calcium.

To derive equations for determining pyroxene compositions from reflectance spectra, spectra need to be measured for compositionally well-characterized pyroxenes. Gaffey et al. (2002) derived a series of equations using spectral data from Adams (1974, 1975) and Cloutis and Gaffey (1991) of compositionally characterized pyroxenes. Gaffey et al. (2002) found that no single equation was applicable to the full range of pyroxene compositions. They found that the wollastonite (Wo) content was a function of the Band I center whereas

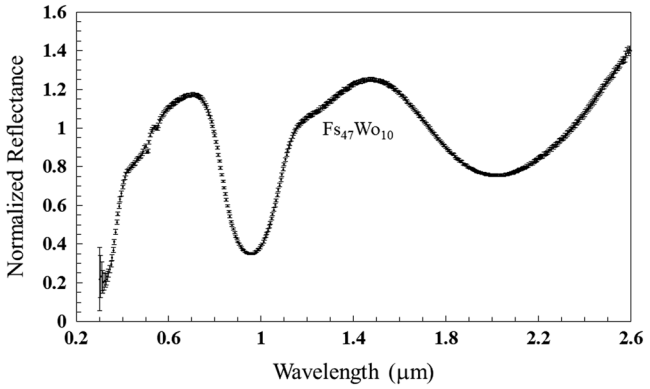

Figure 1. Normalized reflectance spectrum of a synthetic pyroxene with composition $Fs_{47}Wo_{10}$. The spectrum is normalized to unity at 0.55 μm. The error bars are one sigma.

the ferrosilite (Fs) content was a function of the Band II center. Gaffey et al. (2002) derived seven equations, three for calculating the Wo content and four for calculating the Fs content.

Burbine et al. (2009) used the spectra of 13 basaltic achondrites (also known as HEDs [howardites, eucrites, diogenites]) with reflectance spectra (Burbine et al., 2001; Hiroi et al., 1994, 1995) and measured pyroxene compositions to derive formulas for determining the mineralogies of V-type asteroids. V-type asteroids (often called Vestoids) have distinctive spectral features due to pyroxene. V-type asteroids have interpreted mineralogies similar to HEDs (e.g., Kelley et al., 2003), a clan of basaltic meteorites. Asteroid (4) Vesta, the second-largest body in the asteroid belt, is commonly thought to be the parent body of almost all HEDs due to similarities in spectral reflectance (e.g., Larson & Fink, 1975; McCord et al., 1970). Vesta was also one of the targets of the Dawn spacecraft mission (Russell et al., 2012), whose measurements were also consistent with a linkage with HEDs (e.g., McSween et al., 2013). However, some HEDs have distinctly different oxygen isotope values from typical HED values (e.g., Benedix et al., 2017; Scott et al., 2009) implying more than one Vesta-like asteroid formed in the solar system. Hardersen et al. (2018) has determined the pyroxene mineralogies of approximately 30 V-type asteroids in the inner and outer belt to test their mineralogical relationship with Vesta.

Recently, Klima (2008) and Klima et al. (2007, 2008, 2011) did a spectral and mineralogical study of synthetically produced pyroxenes (Turnock et al., 1973; Lindsley, 1983). This study will test whether band centers derived from these synthetic pyroxene reflectance spectra can be used to derive equations for determining the pyroxene mineralogies of V-type asteroids. Alternatively, are equations derived from the band centers of HEDs with known pyroxene compositions better for determining pyroxene mineralogies of V-type asteroids? Our study will investigate how well we can determine V-type pyroxene mineralogies. The pyroxene mineralogies of only V-type NEAs (near-Earth asteroids) will be determined. V-type NEAs have roughly similar sizes (~2 km or less in diameter) and orbits, which will hopefully mean that the studied V-type NEAs will have had roughly similar surface lifetimes and been exposed to similar fluxes of radiation from the Sun.

2. Data and Methodology

The pyroxenes in this study were synthesized by Donald Lindsley and coworkers between 1972 and 2007 using the techniques detailed in Turnock et al. (1973). The samples were prepared from reagent grade chemicals, and the oxygen fugacity was buffered at the iron-wüstite boundary. Specific synthesis methods varied by composition and were chosen to prevent the nucleation of pyroxenoids and to produce a single pyroxene that was homogeneous in composition. Pyroxene mineralogies were validated using X-ray diffraction. Mössbauer spectra were obtained by Klima (2008) on the pyroxene samples, and no samples were found to contain Fe^{3+} or other iron-bearing phases. The powders were crushed and sieved to less than 45 μm and greater than 45 μm grain size fractions for spectroscopic and compositional analysis (Klima, 2008). The less than 45 μm size fraction was used for visible/near-infrared and Mössbauer spectroscopy. The visible/near-infrared spectra were taken at the KECK/NASA Reflectance Experiment Laboratory (RELAB) at Brown University. When available, the greater than 45 μm size fraction was used to prepare grain mounts for electron microprobe analysis where the enstatite (En), ferrosilite (Fs), and wollastonite (Wo) molar contents were determined. The total of the En, Fs, and Wo contents will equal ~100. The pyroxene mineralogies derived from the electron analyses often differed from the mineralogies derived from the X-ray diffraction analyses. The mean difference in Fs content between the probe and the X-ray diffraction results for synthetic pyroxenes used in this study was ~5 mol%, while the mean difference in Wo content was ~3 mol%. Approximately one fourth of the synthetic pyroxenes had differences of 9 mol% differences or greater between the probe and the X-ray diffraction results.

The Band I and II centers and uncertainties for the pyroxene spectra were calculated using a specially written MATLAB™ program that was modified from the one used in Burbine (2014). The primary revisions were to normalize the uncertainties when the reflectance values are normalized to unity during the fitting, to do

Table 1
Band I and Band II Centers With Errors for Synthetic Pyroxene Reflectance Spectra With Measured Compositions Using an Electron Microprobe (Klima, 2008)

	Band II		Band II		(mol%)		
RELAB ID	Center	Error	Center	Error	En	Fs	Wo
DL-CMP-002-A	0.914	0.002	1.875	0.000	80	20	0
DL-CMP-003-A	0.916	0.002	1.895	0.001	77	23	0
DL-CMP-004-A	0.925	0.000	1.969	0.002	50	50	0
DL-CMP-005-A	0.921	0.002	1.948	0.002	43	57	0
DL-CMP-020-A	0.950	0.001	2.043	0.002	18	82	0
DL-CMP-021-A	0.958	0.002	2.061	0.002	9	91	0
DL-CMP-022-A	0.915	0.001	1.890	0.001	75	25	0
DL-CMP-023-A	0.945	0.001	2.020	0.000	30	70	0
DL-CMP-024-A	0.948	0.002	2.045	0.000	18	82	0
DL-CMP-025-A	0.940	0.000	2.010	0.000	35	65	0
DL-CMP-026-A	0.917	0.002	1.909	0.002	72	28	0
DL-CMP-027-A	0.914	0.002	1.875	0.001	80	20	0
DL-CMP-028-A	0.938	0.003	2.025	0.000	25	75	0
DL-CMP-061-A	0.961	0.002	2.065	0.000	0	100	0
DL-CMP-064-A	0.908	0.002	1.817	0.005	97	3	0
DL-CMP-065-A	0.909	0.002	1.838	0.003	90	10	0
DL-CMP-015-A	0.930	0.002	1.908	0.004	79	19	2
DL-CMP-012-A	0.940	0.002	1.961	0.002	62	35	3
DL-CMP-010-A	0.953	0.003	1.976	0.002	73	20	7
DL-CMP-018-A	0.945	0.002	1.944	0.004	78	14	8
DL-CMP-053-A	0.974	0.002	2.100	0.001	23	70	8
DL-CMP-009-A	0.956	0.003	2.055	0.001	43	47	10
DL-CMP-011-A	0.960	0.001	2.068	0.002	36	50	14
DL-CMP-013-A	0.940	0.002	2.011	0.002	56	31	14
DL-CMP-019-A	1.000	0.001	2.186	0.003	69	15	16
DL-CMP-056-A	0.977	0.002	2.121	0.002	18	60	22
DL-CMP-017-A	0.990	0.000	2.176	0.002	65	12	23
DL-CMP-050-A	0.995	0.000	2.140	0.001	19	58	23
DL-CMP-057-A	1.000	0.001	2.238	0.003	36	39	25
DL-CMP-055-A	1.009	0.002	2.195	0.001	18	56	26
DL-CMP-051-A	1.000	0.000	2.200	0.001	39	34	27
DL-CMP-087-A	0.975	0.000	2.210	0.001	0	71	29
DL-CMP-066-A	1.020	0.000	2.240	0.000	15	48	38
DL-CMP-068-A	1.020	0.001	2.246	0.002	29	33	38
DL-CMP-067-A	1.019	0.002	2.287	0.004	52	9	39
DL-CMP-073-A	1.016	0.002	2.298	0.002	36	25	39
DL-CMP-074-A	1.022	0.002	2.260	0.001	24	37	39
DL-CMP-085-A	1.030	0.000	2.264	0.002	0	61	39
DL-CMP-070-A	1.040	0.000	2.258	0.003	14	41	45
DL-CMP-075-A	1.030	0.001	2.290	0.003	46	9	45
DL-CMP-077-A	1.025	0.000	2.300	0.003	52	3	45
DL-CMP-071-A	1.035	0.000	2.290	0.002	23	31	46
DL-CMP-076-A	1.039	0.002	2.295	0.004	18	35	46
DL-CMP-079-A	1.035	0.001	2.297	0.002	38	15	47
DL-CMP-033-A	1.044	0.002	2.315	0.007	42	8	49
DL-CMP-036-A	1.051	0.002	2.297	0.007	27	24	49
DL-CMP-037-A	1.058	0.003	2.326	0.020	16	35	49
DL-CMP-039-A	1.055	0.001	2.319	0.006	29	22	49
DL-CMP-044-A	1.045	0.000	2.309	0.004	43	8	49
DL-CMP-082-A	1.060	0.001	2.309	0.121	1	50	49

Note. The spectra are ordered with increasing wollastonite content. All the spectra were taken of samples of grain sizes of less than 45 μm. No uncertainties were given for the measured En, Fs, and Wo contents. The sum of the En, Fs, and Wo contents sometimes does not equal 100% due to rounding to the nearest integer.

the resampling 99,999 times, and to fit Band I using a fourth order polynomial. Band II is fit with a second-order polynomial; however, Band I is fit with a fourth-order polynomial due to the potentially more complex nature of the band in high-Ca pyroxenes. The broader nature of Band II relative to Band I for these pyroxene-dominated spectra appears visually to allow for a lower order fit to the band. The program inputs the wavelength, reflectance, and the reflectance uncertainties for a spectrum. Fourth-order polynomials were first fit over the maxima at ~0.7, ~1.5, and ~2.5 μm to determine eak positions. The continua over Bands I and II were then divided out using the maxima as tangent points. The bottom one third of Band I was then fit with a fourth-order polynomial and the bottom one third of Band II was then fit with a second-order polynomial. The wavelengths of the band minima were then determined. All reflectance values for the asteroid spectra were then randomly resampled using a Gaussian distribution based on the one-sigma uncertainty for each reflectance value. The resampling produces a new spectrum, which is then fit. This resampling was then done 99,999 times for each band. The goal of the resampling and refitting is to determine the range of possible band centers consistent with the uncertainties of the spectrum. A mean band minimum and a standard deviation for each band can then be determined. All Band I centers and Band II centers, respectively, for the synthetic pyroxene, the meteorite, and the asteroid spectra are fit using the exact same way to allow the calculated band centers for different materials to be directly comparable to each other. Different fitting routines and different polynomial fits will produce different band centers; however, the results using different methods should be comparable as long as all spectra are analyzed the same way.

All available pyroxene spectra were fit. However, the only spectra that were used in this analysis (Table 1) were those that had calculated Band I and Band II centers that fell on a relatively straight curve in a plot of Band I versus Band II center and also were electron microprobed to determine their pyroxene compositions. The band centers for these pyroxenes are plotted in Figure 2. Pyroxenes with Wo_0, which are extremely rare in meteorites, are plotted with different symbols than pyroxenes with $Wo_{>0}$.

To try to determine if these pyroxene spectra can be used to determine the mineralogies of asteroids, the calculated pyroxene band centers and their mineralogies are compared to the band centers and pyroxene mineralogies of 13 HEDs (Table 2) studied by Burbine et al. (2009). Like the synthetic pyroxenes, the HED spectra were measured at RELAB. The pyroxene mineralogies are the average mineralogies of all pyroxenes determined using electron microprobe analyses of thin sections of these meteorites. We do note that the thin sections were not made from the same samples that were used for reflectance spectra. This could potentially be an issue for polymict eucrites and howardites; however, very little research has been done previously on correlating the spectral reflectance and microprobe measurements of HEDs. The band centers for these HEDs are also plotted in Figure 2. The HEDs have band centers that fall on the trend for synthetic pyroxenes. Other researchers (e.g., Beck et al., 2011) have also seen a relatively linear trend for HEDs when their Band II centers versus their Band I centers are plotted. The HED band centers tend to overlap the

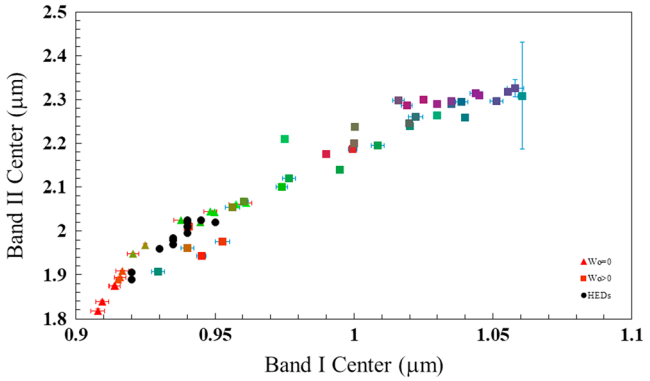

Figure 2. Plot of Band II center versus Band I center for synthetic pyroxenes and HEDs used in this analysis. The squares are used for pyroxenes with $Wo_{>0}$, the triangles are used for pyroxenes with $Wo_{=0}$, and the black circles are used for HEDs. A color gradient is used for the synthetic pyroxene symbols with a pure En composition having a red color, a pure Fs composition having a green color, and a pure Wo composition (which does not exist in nature) having a blue color. Synthetic pyroxenes with intermediate compositions will have colors that are weighted mixtures of red, green, and blue.

points for Wo_0 pyroxenes even though the HED pyroxenes have Wo_{2-14} contents.

Eucrites, diogenites, and howardites are three groups of pyroxene-rich achondritic meteorites (e.g., Mittlefehldt et al., 1998). Almost all members of these groups appear to have been derived from the same parent body due to relationships in mineralogy and chemistry plus similar oxygen isotopic values. Eucrites are primarily composed of anorthite and a low-Ca pyroxene with exsolved lamellae of augite. Diogenites primarily contain Mg-rich orthopyroxene. Howardites are polymict breccias that contain fragments of both eucrites and diogenites. The HED meteorites contain a wide variety of pyroxenes, including orthopyroxene, augite, and pigeonite. These pyroxenes range in composition from the magnesian diogenitic orthopyroxenes to iron-rich pyroxenes of the Nuevo Laredo trend eucrites. The Nuevo Laredo trend is characterized by limited variations of incompatible element contents despite considerable variations in the ratio of magnesium to iron and appears to represent melts that have undergone varying degrees of fractional crystallization (Warren & Jerde, 1987). Pyroxenes also display a wide variety of equilibration textures. Metamorphosed pyroxenes in some HED meteorites are composed of a host of low-Ca pyroxene with augite exsolution lamellae. Unequilibrated eucritic pyroxenes, similar to those found in quickly cooled terrestrial lava flows, have extreme zoning with magnesian cores and iron-rich edges. Even though HEDs contain a wide variety of pyroxenes, HEDs have only one Band I absorption band and one Band II absorption band due to the pyroxenes in the meteorite. However, olivine-bearing diogenites can have their pyroxene band centers influenced by their olivine component (e.g., Carli et al., 2018).

3. Results

Figure 3 plots the Band I center versus the Fs content of the pyroxenes, Figure 4 plots the Band I center versus the Wo content, Figure 5 plots the Band II center versus the Fs content, and Figure 6 plots the Band II center versus the Wo content. The plots of band center versus Wo content (Figures 4 and 6) tend to be relatively linear with longer band centers correlating with increasing Wo content. The plots of band center versus the Fs content (Figures 3 and 5) appear much more complicated. At shorter wavelengths (0.9–0.98 and 1.8–2.1 μm), longer band centers tend to indicate increasing Fs content. However, at wavelengths longer than 0.98 μm for

Table 2
Band I and Band II Centers for HEDs With Measured Pyroxene Mineralogies

		Band I		Band II					
Name	RELAB ID	Center	Error	Center	Error	En	Fs	Wo	Type
Tatahouine	MP-TXH-088-A	0.92	0	1.905	0	75.5	23	1.5	diogenite
Johnstown	MB-TXH-095-A	0.92	0	1.89	0	73.7	23.5	2.8	diogenite
EET 87503	MB-TXH-068-A	0.93	0	1.96	0	51.6	40.3	8.1	howardite
Petersburg	MP-TXH-070-A	0.935	0	1.98	0	50	40.6	9.4	eucrite, polymict
Stannern	MB-TXH-097-A	0.94	0	2.025	0	34.6	55.8	9.6	eucrite, monomict
EETA79005	MP-TXH-072-A	0.935	0	1.97	0	46.5	43.2	10.3	eucrite, polymict
LEW 87004	MP-TXH-079-A	0.935	0	1.985	0	44	45	11	eucrite, polymict
Juvinas	MB-TXH-070-A	0.94	0	1.995	0	36.9	51.8	11.3	eucrite, monomict
EET 87542	MP-TXH-075-A	0.94	0	2.01	0	43	44	13	eucrite, brecciated
EET 90020	MP-TXH-076-A	0.94	0	2.01	0	33	53	13	eucrite, unbrecciated
Pasamonte	MP-TXH-087-A	0.94	0	2.02	0	42.7	43.5	13.7	eucrite, polymict
PCA 82502	MP-TXH-080-A	0.945	0	2.025	0	33	53	14	eucrite, unbrecciated
Bouvante	MP-TXH-090-A	0.95	0	2.02	0	32.5	53.5	14	eucrite, monomict

Note. The uncertainties for the band centers are zero since the errors are not given for their reflectance measurements. The spectra are ordered with increasing wollastonite content. All spectra were measured for grain sizes of less than 25 μm. Petersburg, EET 87542, and EET 90020 were indicated in the RELAB database as being slightly rusted; however, their spectra visually looked not to be influenced by iron oxides.

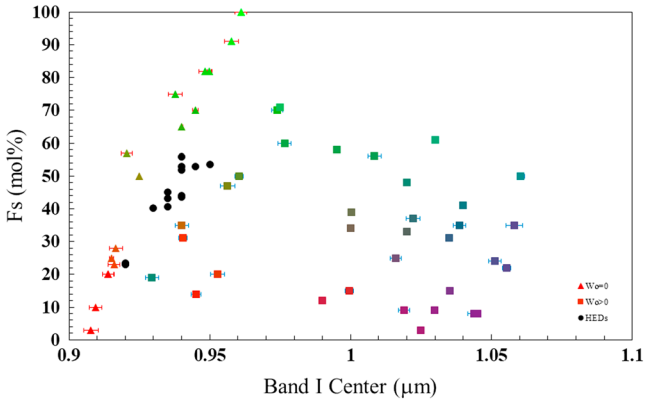

Figure 3. Plot of Fs content (mol%) versus Band I center for synthetic pyroxenes and HEDs. The squares are used for pyroxenes with $Wo_{>0}$, the triangles are used for pyroxenes with $Wo_{=0}$, and the black circles are used for HEDs. A color gradient is used for the synthetic pyroxene symbols with a pure En composition having a red color, a pure Fs composition having a green color, and a pure Wo composition (which does not exist in nature) having a blue color. Synthetic pyroxenes with intermediate compositions will have colors that are weighted mixtures of red, green, and blue.

Band I and 2.1 μm for Band II, there is considerable scatter but with a slight trend of decreasing Fs content for longer band centers.

The HEDs fall on a relatively linear trend but for a much more restricted compositional range than the synthetic pyroxenes in Figures 3–6. However, for the most part, the trend for the HEDs do not overlap well the trends for the $Wo_{>0}$ pyroxenes. The trend for the HEDs tends to fall above the trends for $Wo_{>0}$ pyroxenes. The HED values do not have any error bars since the HED reflectance spectra did not have reflectance points with listed uncertainties.

The reason that trends for $Wo_{>0}$ pyroxenes do not appear able to reliably predict the mineralogies of HED meteorites is that HEDs contain a wide variety of pyroxenes that have differing optical constants. The imaginary index of refraction (*k*), which is a function of wavelength and is related to how efficiently light is absorbed by a medium, varies between pyroxenes of different mineralogies (Fs and Wo contents; Trang et al., 2013). Therefore, the spectral properties of one pyroxene with a particular mineralogy will not be equivalent to the spectral properties of a material containing a variety of pyroxenes with the same average mineralogy as that one pyroxene. Moriarty and Pieters (2016) have previously noted that the relationship between band centers and mineralogy for synthetic pyroxenes is different than the relationship between band centers and mineralogy for naturally occurring pyroxenes. We argue that formulas for deriving asteroid pyroxene mineralogies should be derived from meteoritic spectra with measured compositions since this material will best reflect the compositions of asteroids, which are physical mixtures of a variety of different pyroxenes. Formulas derived from the spectra of just pyroxenes with measured compositions will not accurately predict the pyroxene mineralogies of asteroids. We do note that reflectance spectra of pyroxenes with a single composition are critical for determining optical constants for radiative transfer modeling.

Four linear formulas have been derived to determine the pyroxene mineralogies (Fs and Wo molar contents) of the HEDs. The formulas are

$$Fs\ (mol\%)\ (\pm 4) = 1119.4 \times Band\ I\ Center\ (\mu m) - 1004.1, \quad (1)$$

$$Wo\ (mol\%)\ (\pm 1) = 436.31 \times Band\ I\ Center\ (\mu m) - 398.33, \quad (2)$$

$$Fs\ (mol\%)\ (\pm 3) = 223.15 \times Band\ II\ Center\ (\mu m) - 398.91, \text{and} \quad (3)$$

$$Wo\ (mol\%)\ (\pm 1) = 85.342 \times Band\ II\ Center\ (\mu m) - 159.21. \quad (4)$$

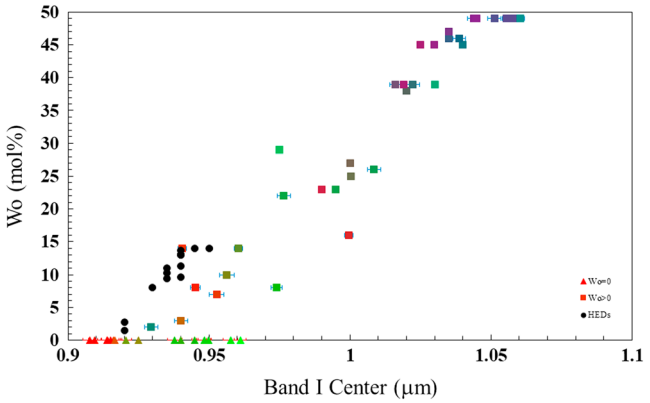

Figure 4. Plot of Wo content (mol%) versus Band I center for synthetic pyroxenes and HEDs. The squares are used for pyroxenes with $Wo_{>0}$, the triangles are used for pyroxenes with $Wo_{=0}$, and the black circles are used for HEDs. A color gradient is used for the synthetic pyroxene symbols with a pure En composition having a red color, a pure Fs composition having a green color, and a pure Wo composition (which does not exist in nature) having a blue color. Synthetic pyroxenes with intermediate compositions will have colors that are weighted mixtures of red, green, and blue.

The uncertainties are calculated by finding the average deviation of the measured molar content versus the predicted content. The R^2 (coefficient of determination) for equation (1) is 0.886, for equation (2) is 0.8485, for equation (3) is 0.8723, and for equation (4) is 0.8652. These newly derived formulas are different than the previously derived formulas of Burbine et al. (2009) even though the same HED reflectance spectra are used. The previously derived formulas are

$$Fs\ (mol\%)\ (\pm 4) = 1023.4 \times Band\ I\ Center\ (\mu m) - 913.82, \quad (5)$$

$$Wo\ (mol\%)\ (\pm 1) = 396.13 \times Band\ I\ Center\ (\mu m) - 360.55, \quad (6)$$

$$Fs\ (mol\%)\ (\pm 3) = 205.86 \times Band\ II\ Center\ (\mu m) - 364.3, \text{and} \quad (7)$$

$$Wo\ (mol\%)\ (\pm 1) = 79.905 \times Band\ II\ Center\ (\mu m) - 148.3. \quad (8)$$

The Burbine et al. (2009) equations are different due to using different fitting techniques for the band centers, which results in slightly

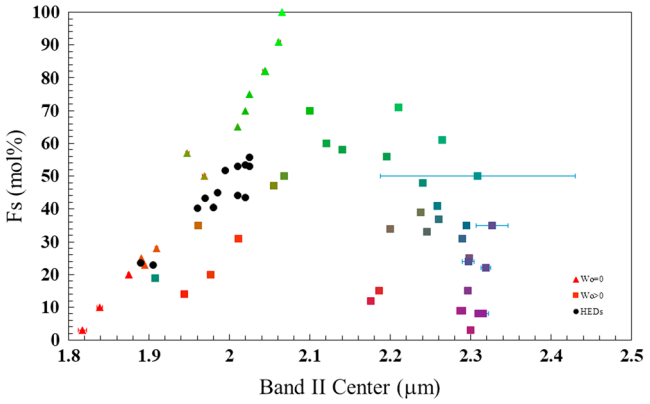

Figure 5. Plot of Fs content (mol%) versus Band II center for synthetic pyroxenes and HEDs. The squares are used for pyroxenes with $Wo_{>0}$, the triangles are used for pyroxenes with $Wo_{=0}$, and the black circles are used for HEDs. A color gradient is used for the synthetic pyroxene symbols with a pure En composition having a red color, a pure Fs composition having a green color, and a pure Wo composition (which does not exist in nature) having a blue color. Synthetic pyroxenes with intermediate compositions will have colors that are weighted mixtures of red, green, and blue.

different calculated values. Neither set of equations should be considered "better" since the differences are just due to different fitting techniques. These equations should be derived again for future studies to account for most likely different fitting technique that will be used in that study.

There are formulas to determine the pyroxene mineralogies from Band I and formulas to determine pyroxene mineralogies from Band II. Burbine et al. (2009) suggested that the Fs and Wo contents, respectively, determined using the Band I and Band II centers should be averaged to minimize the final uncertainty of the calculated results. The advantage of using the Band I formulas is that the Band I wavelength position should be the least influenced by asteroidal temperatures. Temperature is known to affect the band positions for pyroxene reflectance spectra (Roush & Singer, 1987; Singer & Roush, 1985) and shift the band positions to shorter wavelengths at asteroidal temperatures. The estimated temperature corrections to Band I are less than ~ + 0.005 μm for most NEA surface temperatures (~210–270 K; Burbine et al., 2009; Reddy et al., 2012). Almost all meteorite and mineral spectra are only measured at room temperature.

One possible disadvantage of using the Band I formulas is that the Band I wavelength position could be influenced by olivine, which potentially could be found on pyroxene-dominated surfaces. However, pyroxene tends to be more absorbing than olivine so pyroxene tends to dominate the spectral properties of pyroxene-olivine mixtures except for high concentrations of olivine (e.g., Cloutis et al., 1986). Beck et al. (2013) have found from spectral studies of harzburgitic diogenites, which contain Mg-rich pyroxene and olivine, that olivine concentrations of less than ~30% would not noticeably affect the spectral properties of a diogenitic spectrum. The advantage of using the Band II formulas is that the Band II wavelength position would not be expected to be influenced by a relatively small olivine component.

The disadvantage of using the Band II formulas is that the Band II wavelength position is influenced to a larger extent at asteroidal temperatures with estimated temperature corrections of +0.01 to +0.02 μm (Burbine et al., 2009). A howardite measured at 200 and at 300 K for different grain sizes had a Band II temperature correction to room temperature of 0.02–0.03 μm (Burbine et al., 2001). The range (0.03 μm) in measured Band I centers is also much smaller than the range (0.135 μm) in measured Band II centers for the HEDs. Small errors in determining the Band I center will lead to large differences in the estimated Fs and Wo contents.

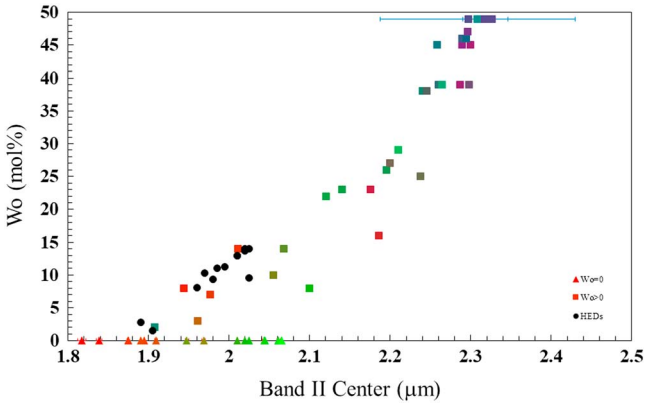

Figure 6. Plot of Wo content (mol%) versus Band II center for synthetic pyroxenes and HEDs. The squares are used for pyroxenes with $Wo_{>0}$, the triangles are used for pyroxenes with $Wo_{=0}$, and the black circles are used for HEDs. A color gradient is used for the synthetic pyroxene symbols with a pure En composition having a red color, a pure Fs composition having a green color, and a pure Wo composition (which does not exist in nature) having a blue color. Synthetic pyroxenes with intermediate compositions will have colors that are weighted mixtures of red, green, and blue.

To do the temperature corrections in the Burbine et al. (2009) study, the results of Moroz et al. (2000), who measured the movement of the band centers for two pyroxenes at temperatures of 293, 173, and 80 K, respectively, were used. One sample ("bronzite") was an orthopyroxene (En_{83}), whereas the other sample ("enstatite") was an orthopyroxene (En_{90}) that possibly could contain a small amount of clinopyroxene. However, the compositions of these pyroxenes are different than the pyroxene compositions of HEDs (Table 2) and these formulas will not be tested in this study. More recently, Reddy et al. (2012) calculated temperature corrections for a eucrite and a howardite (Hinrichs & Lucey, 2002) and for a diogenite (Schade & Wäsch, 1999). The validity of the Reddy et al. (2012) corrections will be investigated in this study.

Pyroxene mineralogies were calculated for 12 V-type NEAs (Table 3 and Figure 7) that were observed as part of the MIT-UH-IRTF Joint Campaign for NEO Spectral Reconnaissance (Binzel et al., 2006). This observing campaign was instituted at the NASA Infrared Telescope Facility (IRTF) to routinely obtain near-infrared reflectance spectra of NEAs. IRTF near-infrared spectra can be used to mineralogically characterize the

Table 3
V-type NEAs Analyzed in This Paper

Name	IRTF observation (UTC) (day/month/year)	Distance to the Sun (AU)	Visual albedo	Estimated surface temperature (K)	Estimated diameter (km)
(1981) Midas	31/10/13	1.301	(0.33)	227	(2.1)
(3908) Nyx	15/9/04	1.153	0.16	255	1.0
(4055) Magellan	11/4/05	1.843	0.341	190	2.1
(5604) 1992 FE	29/3/01	1.258	0.443	220	0.6
(6611) 1993 VW	10/5/05	1.138	0.158	257	1.4
(7889) 1994 LX	7/7/08	1.685	0.552	180	1.7
(8566) 1996 EN	2/9/09	1.022	0.328	256	1.0
(88188) 2000 XH_{44}	20/2/04	1.254	0.236	239	(1.7)
(253841) 2003 YG_{118}	6/2/11	1.135	(0.33)	243	(0.9)
(297418) 2000 SP_{43}	23/10/11	1.173	0.38	234	0.4
(326290) Akhenaten	29/4/12	1.092	(0.33)	247	(0.1)
(480883) 2001 YE_4	30/12/11	1.021	(0.33)	256	(0.2)

Note. Given are the IRTF observation date, distance to the Sun when observed at the IRTF, visual albedo, estimated average surface temperature for the IRTF observation, and estimated diameter.
The albedo and diameter of Nyx are from Benner et al. (2002). The albedos and diameters of Magellan, 1992 FE, and 1996 EN are from Trilling (2018). The albedo and diameter of 1993 VW is from Masiero et al. (2017). The albedos and diameters of 1994 LX and 2000 SP_{43} are from Nugent et al. (2015). The albedo of 2000 XH_{44} is from Pravec et al. (2012). Asteroids without published albedos are given the value of 0.33, which is the average of all the measured V-type NEA albedos in this study. This albedo value is in parentheses for objects without published albedos. The diameters in parentheses are estimated using the object's albedo and H magnitude from the Minor Planet Center database.

asteroid since both olivine and pyroxene absorption features are covered. The near-infrared asteroid spectra were coupled with visible data (Binzel et al., 2001, 2004; de León et al., 2010; Hicks et al., 2011; M. Hicks, personal communication, October 26, 2010) to allow for spectral coverage shorter than ~0.7 μm peak apparent in pyroxene spectra. The visible spectra, which often included some spectral coverage in the

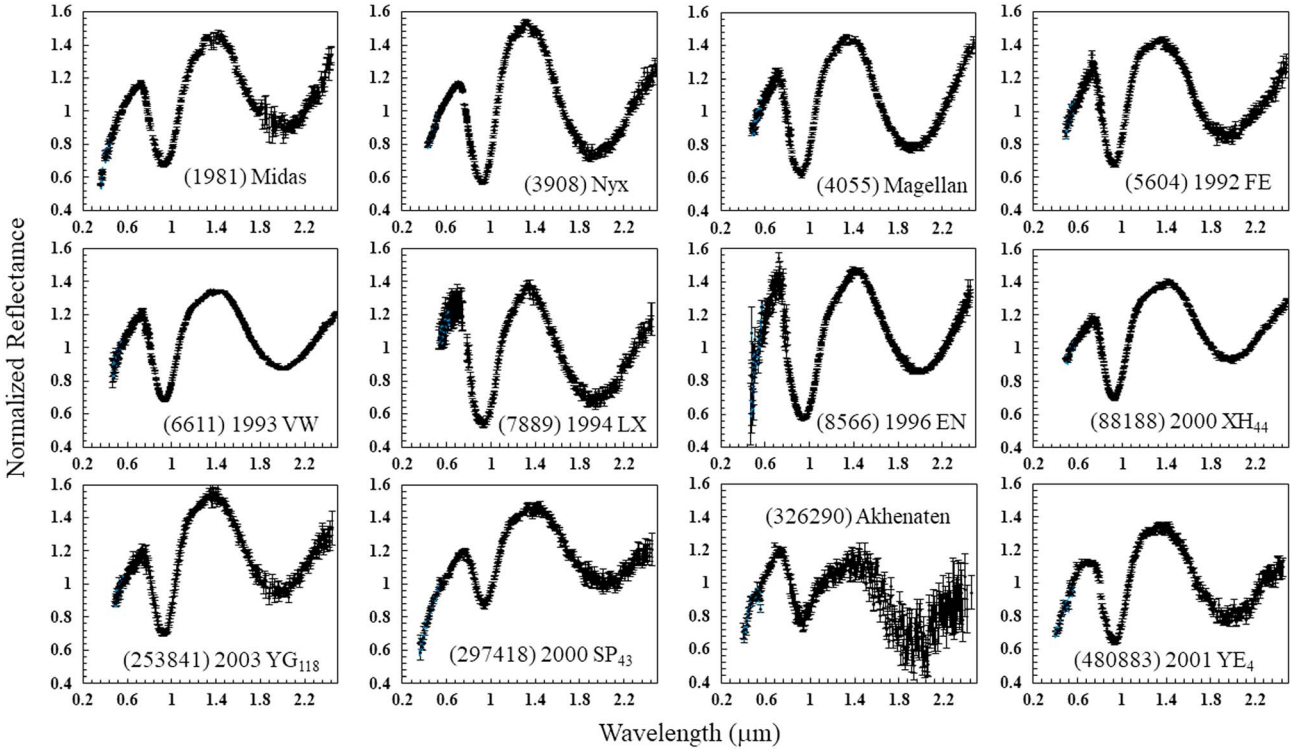

Figure 7. Plots of V-type NEA reflectance spectra. All spectra are normalized to approximately unity at ~0.55 μm. The error bars are one sigma.

Table 4
V-type NEAs That Had Their Band Centers and Errors Calculated

	Band I		Band II		From Band I		From Band II	
Name	Center	Error	Center	Error	Fs	Wo	Fs	Wo
(1981) Midas	0.946	0.002	1.978	0.004	**55**	**14**	42	10
(3908) Nyx	0.935	0.001	1.906	0.002	**42**	**9**	26	3
(4055) Magellan	0.930	0.001	1.930	0.001	**37**	**7**	32	6
(5604) 1992 FE	0.930	0.001	1.920	0.002	**37**	**7**	30	5
(6611) 1993 VW	0.935	0.000	1.975	0.001	**43**	**10**	42	9
(7889) 1994 LX	0.935	0.002	1.908	0.003	**43**	**10**	27	4
(8566) 1996 EN	0.946	0.000	1.981	0.002	**55**	**15**	43	10
(88188) 2000 XH_{44}	0.930	0.001	1.955	0.000	**37**	**7**	37	8
(253841) 2003 YG_{118}	0.938	0.004	1.927	0.003	**45**	**11**	31	5
(297418) 2000 SP_{43}	0.945	0.003	1.972	0.006	**53**	**14**	41	9
(326290) Akhenaten	0.917	0.012	1.932	0.017	**22**	**2**	32	6
(480883) 2001 YE_4	0.936	0.003	1.948	0.005	**44**	**10**	36	7

Note. The pyroxene mineralogies calculated from the Band I center and also from the Band II center are given. The values in bold are our best estimates for the average pyroxene mineralogies of the V-type NEAs. The average mineralogies are calculated using more significant digits than the given band centers. The uncertainty for the Fs content derived from the Band I center is ±4 mol%, the uncertainty for the Wo content derived from the Band I center is ±1 mol%, the uncertainty for the Fs content derived from the Band II center is ±3 mol%, and the uncertainty for the Wo content derived from the Band II center is ±1 mol%.

near-infrared and ultraviolet, were obtained using various telescopes. We note that the visible and IRTF spectra of the same object were all taken at different times. Observation and reduction details for IRTF observations are discussed in Binzel et al. (2001). All these V-type reflectance spectra had spectral properties similar to HEDs. All V-type NEA spectra were fit in the same manner as the fitting for the synthetic pyroxenes and HEDs. Any overlapping data points in wavelength due to combining two telescopic observations were deleted from the shorter wavelength observations. When a long wavelength point at 2.45 μm was added to the spectrum to allow the spectrum to be taxonomically characterized using the web-based Bus-DeMeo classifier, this point was deleted before the fitting.

Space weathering is assumed not to be altering the spectral properties of the V-type asteroids. Blewett et al. (2016) found no evidence for lunar-style space weathering on the surface of Vesta. They used radiative transfer modeling of howardite reflectance spectra with a nanophase iron component to try to duplicate Dawn Framing Camera multispectral observations of Vesta. They were unable to duplicate the spectral differences between fresh and mature areas on the surface. Since the studied V-type asteroids would be expected to have much younger surface ages than Vesta, we assume that space weathering is not affecting the spectral properties of these bodies.

Average surface temperatures, assuming that the asteroid is a gray body heated by the Sun, are calculated for each asteroid using the object's distance from the Sun during its IRTF observation and its visual geometric albedo (calculated or estimated). The temperature is calculated using the formula

$$T = \sqrt[4]{L_o(1-A)/16\pi r^2 \varepsilon \sigma} \tag{9}$$

where L_o is the solar luminosity, A is the visual geometric albedo, r is the asteroid's distance from the Sun, ε is the emissivity (assumed to be 0.9), and σ is the Stefan-Boltzman constant.

Band centers and errors were calculated for the V-type NEAs (Table 4). Also listed are the calculated average pyroxene mineralogies using the Band I and the Band II centers for each object. The Band I and Band II center positions have not been corrected for temperature. The lack of a temperature correction for Band II is readily apparent since the pyroxene mineralogies that are calculated using the Band II center for the V-types are lower than the pyroxene mineralogies calculated using the Band I center for all but two of the objects. A positive temperature correction for Band II would increase the calculated Fs and Wo content for that band center. However, a plot (Figure 8) of the differences in both Fs (black squares) and Wo contents (orange squares) using the band center formulas does not show an obvious trend of decreasing differences in estimated mineralogy with increasing temperature as would be expected.

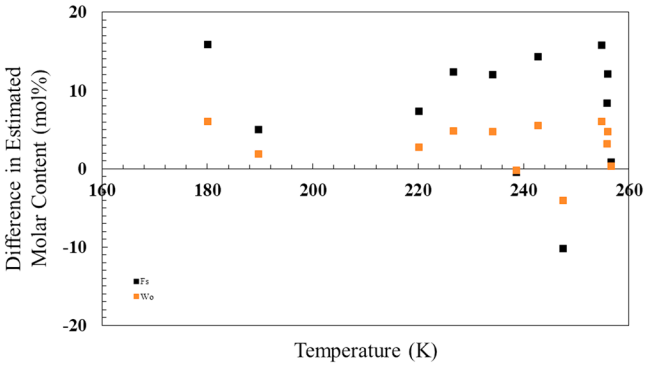

Figure 8. Plot of the differences in Fs (black squares) and Wo contents (orange squares) using the band center formulas. The Fs content from the Band I center formulas is subtracted from the Fs content from the Band II center formula, and the Wo content from the Band I center formulas is subtracted from the Wo content from the Band II center formula.

To investigate whether the movement of the band centers due to temperature can be accurately corrected for, we compare (Figure 9) the band centers for the HEDs versus those for the V-type NEAs before and after a temperature correction. We assume that accurate temperature corrections would shift the trend for the V-type NEAs so the asteroid trend overlaps the trend for the HEDS. We first do a linear regression through the HED values and a weighted linear regression (Thirumalai et al., 2011) through the V-type NEA points to account for the different uncertainty values for some of NEA band centers. For NEA band centers without an uncertainty, we assume an extremely small uncertainty value. The regression lines for the HEDs (R^2 of 0.900) and V-type NEAs (R^2 of 0.900) are roughly parallel but offset. We note that the R^2 for the V-type NEA regression line is very low (0.230) due to the large amount of scatter for the NEA band centers. We then use the temperature correction formulas derived by Reddy et al. (2012) for the V-type NEAs to attempt to correct for the low surface temperatures of the NEAs. For surface temperatures of T (K), the temperature corrections for eucrites/howardites are

$$\text{Band I center correction } (\mu\text{m}) = 0.01656–0.0000552\times\text{T (K)} \tag{10}$$

and

$$\text{Band II center correction } (\mu\text{m}) = 0.05067–0.00017\times\text{T (K)} \tag{11}$$

and for diogenites are

$$\text{Band I center correction } (\mu\text{m}) = 0.0000000017\times\text{T}^3\text{(K)}–0.0000012602\times\text{T}^2\text{(K)} + 0.0002664351\times\text{T (K)}–0.0124 \tag{12}$$

and

$$\text{Band II center correction } (\mu\text{m}) = 0.038544–0.000128\times\text{T (K)}. \tag{13}$$

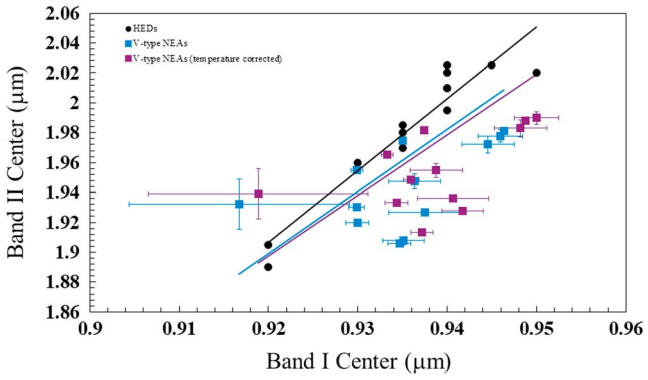

Figure 9. Plot of Band II center versus Band I center for HEDs (black circles), V-type NEAs before the Reddy et al. (2012) temperature correction (blue squares), and V-type NEAs after the Reddy et al. (2012) temperature correction (purple squares). The error bars are one-sigma. The black line is the linear regression through the HED values, the blue line is the weighted linear regression through the V-type NEA values before the temperature correction, and the purple line is the weighted linear regression through the V-type NEA values after the temperature correction. Note that the temperature correction does not significantly move the temperature-corrected V-type NEA weighted regression line toward the HED regression line.

We apply the eucrite/howardite temperature corrections to all the V-type NEA band centers except for Akhenaten where we apply the diogenite temperature corrections due to Akhenaten having band centers more consistent with a diogenite surface mineralogy. We then do a weighted linear regression through the temperature-corrected NEA band centers. The R^2 for the V-type NEA regression line through the temperature-corrected line is still very low (0.178). Interestingly, temperature corrections to both the Band I and II centers do not significantly shift the regression line for the NEA V-type band centers toward the HED regression line. The temperature corrections of Reddy et al. (2012) to both the Band I and II centers tend to shift the V-type NEA band centers parallel to the HED line. For the regression line for the temperature-corrected V-type band centers to overlap the HED regression line, the Band II centers for the NEAs would need to be corrected on average by ~0.02 μm. We note that Hardersen et al. (2018) found a much better correlation between the trend for HEDs and the trend for inner-belt V-types after a temperature correction in a plot of Band II versus Band I centers.

Since it does not appear possible to currently construct an accurate temperature correction for each asteroid based on current laboratory measurements, formulas using only the Band I centers [equations (1)

Table 5
Interpreted Mineralogies of the V-Type Asteroids

Name	Pyroxene mineralogy		Optimistic interpretation	Pessimistic interpretation	Other interpretations
	Fs	Wo			
(1981) Midas	55	14	eucrite	eucrite	eucrite
(3908) Nyx	42	9	howardite	polymict eucrite/howardite	howardite, eucrite
(4055) Magellan	37	7	howardite	polymict eucrite/howardite	howardite, eucrite
(5604) 1992 FE	37	7	howardite	polymict eucrite/howardite	howardite
(6611) 1993 VW	43	10	polymict eucrite	polymict eucrite/howardite	howardite, eucrite
(7889) 1994 LX	43	10	polymict eucrite	polymict eucrite/howardite	eucrite
(8566) 1996 EN	55	15	eucrite	eucrite	
(88188) 2000 XH_{44}	37	7	howardite	polymict eucrite/howardite	
(253841) 2003 YG_{118}	45	11	polymict eucrite	polymict eucrite/howardite	
(297418) 2000 SP_{43}	53	14	eucrite	eucrite	
(326290) Akhenaten	22	2	diogenite	howardite/diogenite	
(480883) 2001 YE_4	44	10	polymict eucrite	polymict eucrite/howardite	

Note. The pyroxene mineralogy is calculated from Band I. The optimistic interpretation takes the pyroxene mineralogy at face, while the pessimistic interpretations takes into account the uncertainties of the measurements and equations. The uncertainty for the given Fs content, which is derived from the Band I center, is ±4 mol%, and the uncertainty for the given Wo content, which is derived from the Band I center, is ±1 mol%.
Batista et al. (2014) found that the best spectral matches for Nyx, Magellan, 1992 FE, and 1993 WW were howardites. Ieva et al. (2016) argued that Midas, Nyx, Magellan, 1993 VW, and 1994 LX had surface mineralogies similar to eucrites.

and (2)] are used to estimate the mineralogies of the V-type NEAs. If you take the derived mineralogies at face value (Table 5), Akhenaten has a composition similar to diogenites due to its calculated magnesian, low-Wo content that is similar to Johnstown or Tatahouine. Midas, 1996 EN, and 2000 SP_{43} appear relatively Fe-rich and seem to be most similar to Bouvante or PCA 82502. Bouvante is the most rare earth element-rich of the "classical" eucrites," indicating a low degree of partial melting (e.g., Barrat et al., 2007). PCA 82502 is a fine-grained, light rare earth element-depleted, unbrecciated eucrite with a low degree of equilibration and is argued to have erupted as a surface flow (Bermingham et al., 2008). Paniello et al. (2012) argues that PCA 82502 is from a distinct parent body compared to other HEDs due to extremely light zinc isotopic composition. Fe-rich eucrites are either highly differentiated (e.g., Nuevo Laredo) or represent a lower degree of partial melting (e.g., Bouvante, Stannern; e.g., Mittlefehldt, 1992) than Main Group eucrites (e.g., Juvinas; e.g., Stolper, 1975). The other V-type NEAs seem to be most similar to polymict breccias (polymict eucrites or howardites). We note that discriminating between the howardites and polymict eucrites is a bit more difficult because there is a lot of overlap in composition since both types of meteorites are physical mixtures of eucritic and diogenitic material. However, Nyx, Magellan, 1992 FE, and 2000 XH_{44} appear more like howardites because they are lower in Fs and Wo, which would indicate more of a low-Ca, magnesian diogenitic component. Analogous meteorites would be EET 87503 or EET 87513, which have been proposed to be very similar or paired (e.g., Buchanan & Mittlefehldt, 2003). NEAs 1993 VW, 1994 LX, 2003 YG_{118}, and 2001 YE_4 appear richer in Fe and Wo, which suggests that they might be more like polymict eucrites with less of a low-Ca, magnesian diogenitic component. Analogous meteorites would be EETA79005 or LEW 87004. It is also possible that these NEAs with mineralogies similar to polymict meteorites could be similar to a magnesium-rich monomict eucrite (Mittlefehldt & Lindstrom, 1997) or a crystallized impact melt of a eucrite/diogenite mixture.

There is no obvious correlation between diameter (Table 3) and interpreted composition (Table 5). The largest NEAs have either interpreted mineralogies similar to eucrites (e.g., Midas) or howardites (e.g., Magellan). The most interesting possible trend is that Akhenaten, which is the only body with an interpreted diogentic surface mineralogy, has the smallest estimated diameter (~100 m; Table 3) of all the observed NEAs. However, more V-type NEAs would need to be studied to see if diogenitic surface mineralogies are more prevalent at this size.

A more pessimistic (and probably more realistic) interpretation (Table 5) that takes in all the uncertainties of the measurements and equations would be that Akhenaten has a diogenite or howardite composition. Midas, 1996 EN, and 2000 SP_{43} are most similar to some type of eucrite. Nyx, Magellan, 1992 FE, 1993 VW, 1994 LX, 2000 XH_{44}, 2003 YG_{118}, and 2001 YE_4 are either polymict eucrites or howardites. Without any

ground truth (a sample from a characterized body), these general meteoritic interpretations are the most defendable using the derived formulas. However, if the same specific meteoritic interpretation was verified using a second technique (e.g., absorption band modeling and radiative transfer modeling), more specific interpretations would be much more easily justified. For example, Batista et al. (2014) found that the best spectral matches for Nyx, Magellan, 1992 FE, and 1993 WW were howardites. Ieva et al. (2016) used a number of spectral parameters that they derived from both HEDs and V-types and argued that Midas, Nyx, Magellan, 1993 VW, and 1994 LX had surface mineralogies similar to eucrites.

4. Conclusions

We have tested whether the reflectance spectra of synthetic pyroxenes and/or HEDs with known compositions can be used to determine the pyroxene mineralogies of V-type NEAs. Our conclusions are the following:

1. Band centers from the reflectance spectra of synthetic pyroxenes with known compositions cannot be used to derive equations for determining accurate pyroxene compositions of V-type asteroids. These V-type asteroids, as apparent by studies of HEDs, contain a wide variety of pyroxenes. Since the absorptions of these different pyroxenes may not vary linearly according to composition, the spectral properties of one pyroxene with a particular mineralogy may not be equivalent to the spectral properties of a material containing a variety of pyroxenes that have the same average mineralogy.
2. Band centers from the reflectance spectra of HEDs with known pyroxene compositions can potentially be used to derive equations for determining accurate pyroxene compositions of V-type asteroids. HEDs are physical mixtures of a number of different types of pyroxenes. HEDs should be analogous to the surface mineralogies of V-type asteroids. Pyroxene analyses coupled with spectral reflectance measurements should be done for more HEDs. One promising technique to do these types of analyses was explored by Fraeman et al. (2016). They did visible-short wavelength infrared imaging spectroscopy of HED fragments at 80 μm/pixel and plan to do spatially correlated scanning electron microscope/energy-dispersive X-ray spectroscopy to determine the mineralogy of every small area on the chip where a spectrum was obtained.
3. Formulas from previous studies should be derived again if the fitting technique used to determine band centers is different at all in the new study. Each different fitting technique most likely will calculate slightly different band centers.
4. Formulas using the Band I center appear best for determining asteroid pyroxene mineralogies for V-type asteroids due to the current difficulty in doing accurate temperature corrections to the Band II Center. More HEDs need to be measured at asteroidal temperatures to derive accurate temperature corrections.
5. Most of these observed V-type NEA have interpreted mineralogies similar to eucrites or howardites. One of the observed NEAs could possibly have a surface mineralogy similar to diogenites.
6. Specific meteoritic interpretations are difficult to conclusively justify without the use of a second technique to validate the interpreted mineralogies of the asteroids.

Acknowledgments
The authors would like to thank Editor David Baratoux and reviewers Pierre Beck and Paul Hardersen for helping to make this paper significantly better. T. H. B. would like to thank the Remote, In Situ, and Synchrotron Studies for Science and Exploration (RIS^{4}E) Solar System Exploration Research Virtual Institute (SSERVI) for support. R. P. B. and T. H. B. would also like to thank NASA grant NAG5-12355 for support for this research. Part of the data utilized in this publication were obtained and made available by the MIT-UH-IRTF Joint Campaign for NEO Reconnaissance. The IRTF is operated by the University of Hawaii under Cooperative Agreement NCC 5-538 with the National Aeronautics and Space Administration, Office of Space Science, Planetary Astronomy Program. The MIT component of this work is supported by NASA grant 09-NEOO009-0001 and by the National Science Foundation under grants 0506716 and 0907766. Mineral and meteorite spectra are available at the RELAB website (http://www.planetary.brown.edu/relabdata/). The near-Earth asteroid IRTF spectra are available at the SMASS website (http://smass.mit.edu/catalog.php). The MATLAB™ code for calculating band centers can be found at http://www.tomburbine.com/matlab.html. The authors would also like to thank Kaustubh Thirumalai for supplying the MATLAB™ code for doing the weighted linear regression.

References

Adams, J. B. (1974). Visible and near-infrared diffuse reflectance spectra of pyroxenes as applied to remote sensing of solid objects in the solar system. *Journal of Geophysical Research*, *79*(32), 4829–4836. https://doi.org/10.1029/JB079i032p04829

Adams, J. B. (1975). Interpretation of visible and near-infrared diffuse reflectance spectra of pyroxenes and other rock-forming minerals. In C. Karr (Ed.), *Infrared and Raman Spectroscopy of Lunar and Terrestrial Minerals* (pp. 91–116). New York, NY: Academic Press. https://doi.org/10.1016/B978-0-12-399950-4.50009-4

Barrat, J. A., Yamaguchi, A., Greenwood, R. C., Bohn, M., Cotten, J., Benoit, M., & Franchi, I. A. (2007). The Stannern trend eucrites: Contamination of main group eucritic magmas by crustal partial melts. *Geochimica et Cosmochimica Acta*, *71*(16), 4108–4124. https://doi.org/10.1016/j.gca.2007.06.001

Batista, S. F. A., Seixas, T. M., Salgueiro da Silva, M. A., & de Albuquerque, R. M. G. (2014). Mineralogy of V-type asteroids as a constraining tool of their past history. *Planetary and Space Science*, *104*(B), 295–309. https://doi.org/10.1016/j.pss.2014.10.012

Beck, A. W., McCoy, T. J., Sunshine, J. M., Viviano, C. E., Corrigan, C. M., Hiroi, T., & Mayne, R. G. (2013). Challenges in detecting olivine on the surface of 4 Vesta. *Meteoritics & Planetary Science*, *48*(11), 2155–2165. https://doi.org/10.1111/maps.12160

Beck, P., Barrat, J.-A., Grisolle, F., Quirico, E., Schmitt, B., Moynier, F., et al. (2011). NIR spectral trends of HED meteorites: Can we discriminate between the magmatic evolution, mechanical mixing and observation geometry effects? *Icarus*, *216*(2), 560–571. https://doi.org/10.1016/j.icarus.2011.09.015

Benedix, G. K., Bland, P. A., Friedrich, J. M., Mittlefehldt, D. W., Sanborn, M. E., Yin, Q.-Z., et al. (2017). Bunburra Rockhole: Exploring the geology of a new differentiated asteroid. *Geochimica et Cosmochimica Acta*, *208*, 145–159. https://doi.org/10.1016/j.gca.2017.03.030

Benner, L. A. M., Ostro, S. J., Hudson, R. S., Rosema, K. D., Jurgens, R. F., Yeomans, D. K., et al. (2002). Radar observations of asteroid 3908 Nyx. *Icarus*, *158*(2), 379–388. https://doi.org/10.1006/icar.2002.6869

Bermingham, K. R., Norman, M. D., Christy, A. G., & Arculus, R. J. (2008). A new variety of eucrite? Clues to early differentiation of igneous asteroids. Lunar and Planetary Science Conference, XXXIX, 1225.

Binzel, R. P., Harris, A. W., Bus, S. J., & Burbine, T. H. (2001). Spectral properties of near-Earth objects: Palomar and IRTF results for 48 objects including spacecraft targets (9969) Braille and (10302) 1989 ML. *Icarus*, *151*(2), 139–149. https://doi.org/10.1006/icar.2001.6613

Binzel, R. P., Rivkin, A. S., Stuart, J. S., Harris, A. W., Bus, S. J., & Burbine, T. H. (2004). Observed spectral properties of near-Earth objects: Results for population distribution, source regions, and space weathering processes. *Icarus*, *170*(2), 259–294. https://doi.org/10.1016/j.icarus.2004.04.004

Binzel, R. P., Thomas, C. A., DeMeo, F. E., Tokunaga, A., Rivkin, A. S., & Bus, S. J. (2006). The MIT-Hawaii-IRTF joint campaign for NEO spectral reconnaissance. Lunar and Planetary Science Conference, XXXVII, 1491.

Blewett, D. T., Denevi, B. W., Le Corre, L., Reddy, V., Schröder, S. E., Pieters, C. M., et al. (2016). Optical space weathering on Vesta: Radiative-transfer models and Dawn observations. *Icarus*, *265*, 161–174. https://doi.org/10.1016/j.icarus.2015.10.012

Buchanan, P. C., & Mittlefehldt, D. W. (2003). Lithic components in the paired howardites EET 87503 and EET 87513: Characterization of the regolith of 4 Vesta. *Antarctic Meteorite Research*, *16*, 128–151.

Burbine, T. H. (2014). Determining band centers from asteroid spectra. Lunar and Planetary Science Conference, 45, 1646.

Burbine, T. H., Buchanan, P. C., Binzel, R. P., Bus, S. J., Hiroi, T., Hinrichs, J. L., et al. (2001). Vesta, Vestoids, and the HEDs: Relationships and the origin of spectral differences. *Meteoritics & Planetary Science*, *36*(6), 761–781. https://doi.org/10.1111/j.1945-5100.2001.tb01915.x

Burbine, T. H., Buchanan, P. C., Dolkar, T., & Binzel, R. P. (2009). Pyroxene mineralogies of near-Earth Vestoids. *Meteoritics & Planetary Science*, *44*(9), 1331–1341. https://doi.org/10.1111/j.1945-5100.2009.tb01225.x

Carli, C., Pratesi, G., Moggi-Cecchi, V., Zambon, F., Capaccioni, F., & Santoro, S. (2018). Northwest Africa 6232: Visible–near infrared reflectance spectra variability of an olivine diogenite. *Meteoritics & Planetary Science*, *53*. https://doi.org/10.1111/maps.13056

Chapman, C. R., & Salisbury, J. W. (1973). Comparisons of meteorite and asteroid spectral reflectivities. *Icarus*, *19*(4), 507–522. https://doi.org/10.1016/0019-1035(73)90078-X

Cloutis, E. A., & Gaffey, M. J. (1991). Pyroxene spectroscopy revisited: Spectral-compositional correlations and relationship to geothermometry. *Journal of Geophysical Research*, *96*(E5), 22,809–22,826. https://doi.org/10.1029/91JE02512

Cloutis, E. A., Gaffey, M. J., Jackowski, T. L., & Reed, K. L. (1986). Calibrations of phase abundance, composition, and particle size distribution for olivine-orthopyroxene mixtures from reflectance spectra. *Journal of Geophysical Research*, *91*(B11), 11,641–11,653. https://doi.org/10.1029/JB091iB11p11641

de León, J., Licandro, J., Serra-Ricart, M., Pinilla-Alonso, N., & Campins, H. (2010). Observations, compositional, and physical characterization of near-Earth and Mars-crosser asteroids from a spectroscopic survey. *Astronomy and Astrophysics*, *517*, A23. https://doi.org/10.1051/0004-6361/200913852

Dunn, T. L., McCoy, T. J., Sunshine, J. M., & McSween, H. Y. Jr. (2010). A coordinated spectral, mineralogical, and compositional study of ordinary chondrites. *Icarus*, *208*(2), 789–797. https://doi.org/10.1016/j.icarus.2010.02.016

Fraeman, A. A., Ehlmann, B. L., Northwood-Smith, G. W. D., Liu, Y., Wadhwa, M., & Greenberger, R. N. (2016). Using VSWIR microimaging spectroscopy to explore the mineralogical diversity of HED meteorites. In *2016 8th Workshop on Hyperspectral Image and Signal Processing: Evolution in Remote Sensing (WHISPERS)* (pp. 1–5). Piscataway, NJ: IEEE. https://doi.org/10.1109/WHISPERS.2016.8071804

Gaffey, M. J., Cloutis, E. A., Kelley, M. S., & Reed, K. L. (2002). Mineralogy of asteroids. In W. Bottke, A. Cellino, P. Paolicchi, & R. P. Binzel (Eds.), *Asteroids III* (pp. 183–204). Tucson, AZ: University of Arizona Press.

Hardersen, P. S., Reddy, V., Cloutis, E., Nowinski, M., Dievendorf, M., Genet, R. M., et al. (2018). Basalt or not? Near-infrared spectra, surface mineralogical estimates, and meteorite analogs for 33 Vp-type asteroids. *The Astronomical Journal*, *156*(1), 11. https://doi.org/10.3847/1538-3881/aac3d2

Hicks, M., Gerhart, C., Stojia, C., & Teague, S. (2011). Palomar spectroscopy of near-Earth asteroids 2004 SV55, 2000 SP43, 3988 (1986 LA), 1036 Ganymed, and 2002 AG29. The Astronomer's Telegram, 3678. Retrieved from http://www.astronomerstelegram.org/?read=3678

Hinrichs, J. L., & Lucey, P. G. (2002). Temperature-dependent near-infrared spectral properties of minerals, meteorites, and lunar soil. *Icarus*, *155*(1), 169–180.

Hiroi, T., Binzel, R. P., Sunshine, J. M., Pieters, C. M., & Takeda, H. (1995). Grain sizes and mineral compositions of surface regoliths of Vesta-like asteroids. *Icarus*, *115*(2), 374–386. https://doi.org/10.1006/icar.1995.1105

Hiroi, T., Pieters, C. M., & Takeda, H. (1994). Grain size of the surface regolith of asteroid 4 Vesta estimated from its reflectance spectrum in comparison with HED meteorites. *Meteoritics*, *29*(3), 394–396. https://doi.org/10.1111/j.1945-5100.1994.tb00603.x

Ieva, S., Dotto, E., Lazzaro, D., Perna, D., Fulvio, D., & Fulchignoni, M. (2016). Spectral characterization of V-type asteroids—II. A statistical analysis. *Monthly Notices of the Royal Astronomical Society*, *455*(3), 2871–2888. https://doi.org/10.1093/mnras/stv2510

Kelley, M. S., Vilas, F., Gaffey, M. J., & Abell, P. A. (2003). Quantified mineralogical evidence for a common origin of 1929 Kollaa with 4 Vesta and the HED meteorites. *Icarus*, *165*(1), 215–218. https://doi.org/10.1016/S0019-1035(03)00149-0

Klima, R. L., Dyar, M. D., & Pieters, C. M. (2011). Near-infrared spectra of clinopyroxenes: Effects of calcium content and crystal structure. *Meteoritics & Planetary Science*, *46*(3), 379–395. https://doi.org/10.1111/j.1945-5100.2010.01158.x

Klima, R. L., Pieters, C. M., & Dyar, M. D. (2007). Spectroscopy of synthetic Mg-Fe pyroxenes I: Spin-allowed and spin-forbidden crystal field bands in the visible and near-infrared. *Meteoritics & Planetary Science*, *42*(2), 235–253. https://doi.org/10.1111/j.1945-5100.2007.tb00230.x

Klima, R. L., Pieters, C. M., & Dyar, M. D. (2008). Characterization of the 1.2 μm M1 pyroxene band: Extracting cooling history from near-IR spectra of pyroxenes and pyroxene-dominated rocks. *Meteoritics & Planetary Science*, *43*(10), 1591–1604. https://doi.org/10.1111/j.1945-5100.2008.tb00631.x

Klima, R. L. P. (2008). Integrated spectroscopy of magnesium-iron-calcium pyroxenes: A foundation for modern remote compositional analysis of planetary surfaces, (Doctoral dissertation). Providence, RI: Brown University.

Larson, H. P., & Fink, U. (1975). Infrared spectral observations of asteroid 4 Vesta. *Icarus*, *26*(4), 420–427. https://doi.org/10.1016/0019-1035(75)90109-8

Lawrence, S. J., & Lucey, P. G. (2007). Radiative transfer mixing models of meteoritic assemblages. *Journal of Geophysical Research*, *112*, E07005. https://doi.org/10.1029/2006JE002765

Lindsley, D. H. (1983). Pyroxene thermometry. *American Mineralogist*, *68*, 477–493.

Masiero, J. R., Nugent, C., Mainzer, A. K., Wright, E. L., Bauer, J. M., Cutri, R. M., et al. (2017). NEOWISE reactivation mission year three: Asteroid diameters and albedos. *The Astronomical Journal*, *154*(4), 168. https://doi.org/10.3847/1538-3881/aa89ec

McCord, T. B., Adams, J. B., & Johnson, T. V. (1970). Asteroid Vesta: Spectral reflectivity and compositional implications. *Science*, *168*(3938), 1445–1447. https://doi.org/10.1126/science.168.3938.1445

McSween, H. Y., Binzel, R. P., de Sanctis, M. C., Ammannito, E., Prettyman, T. H., Beck, A. W., et al. (2013). Dawn; the Vesta-HED connection; and the geologic context for eucrites, diogenites, and howardites. *Meteoritics and Planetary Science*, *48*(11), 2090–2104. https://doi.org/10.1111/maps.12108

Mittlefehldt, D. W. (1992). Petrogenesis of eucrites. *Meteoritics*, *27*(3), 261.

Mittlefehldt, D. W., & Lindstrom, M. M. (1997). Magnesian basalt clasts from the EET 92014 and Kapoeta howardites and a discussion of alleged primary magnesian HED basalts. *Geochimica et Cosmochimica Acta*, *61*(2), 453–462. https://doi.org/10.1016/S0016-7037(96)00357-2

Mittlefehldt, D. W., McCoy, T. J., Goodrich, C. A., & Kracher, A. (1998). Non-chondritic meteorites from asteroidal bodies. In J. J. Papike (Ed.), *Planetary Materials, Reviews in Mineralogy and Geochemistry* (Vol. 68, pp. 4–1–4-195). Washington, DC: Mineralogical Society of America.

Moriarty, D. P., & Pieters, C. M. (2016). Complexities in pyroxene compositions derived from absorption band centers: Examples from Apollo samples, HED meteorites, synthetic pure pyroxenes, and remote sensing data. *Meteoritics & Planetary Science*, *51*(2), 207–234. https://doi.org/10.1111/maps.12588

Moroz, L., Schade, U., & Wäsch, R. (2000). Reflectance spectra of olivine–orthopyroxene-bearing assemblages at decreased temperatures: Implications for remote sensing of asteroids. *Icarus*, *147*(1), 79–93. https://doi.org/10.1006/icar.2000.6430

Nugent, C. R., Mainzer, A., Masiero, J., Bauer, J., Cutri, R. M., Grav, T., et al. (2015). NEOWISE Reactivation Mission Year One: Preliminary asteroid diameters and albedos. *The Astrophysical Journal*, *814*(2), 117. https://doi.org/10.1088/0004-637X/814/2/117

Paniello, R. C., Moynier, F., Beck, P., Barrat, J.-A., Podosek, F. A., & Pichat, S. (2012). Zinc isotopes in HEDs: Clues to the formation of 4-Vesta, and the unique composition of Pecora Escarpment 82502. *Geochimica et Cosmochimica Acta*, *86*, 76–87. https://doi.org/10.1016/j.gca.2012.01.045

Pravec, P., Harris, A. W., Kušnirák, P., Galád, A., & Hornoch, K. (2012). Absolute magnitudes of asteroids and a revision of asteroid albedo estimates from WISE thermal observations. *Icarus*, *221*(1), 365–387. https://doi.org/10.1016/j.icarus.2012.07.026

Reddy, V., Sanchez, J. A., Nathues, A., Moskovitz, N. A., Li, J.-Y., Cloutis, E. A., et al. (2012). Photometric, spectral phase and temperature effects on 4 Vesta and HED meteorites: Implications for the Dawn mission. *Icarus*, *217*(1), 153–168. https://doi.org/10.1016/j.icarus.2011.10.010

Roush, T. L., & Singer, R. B. (1987). Possible temperature variations effects on the interpretation of spatially resolved reflectance observations of asteroid surfaces. *Icarus*, *69*(3), 571–574. https://doi.org/10.1016/0019-1035(87)90026-1

Russell, C. T., Raymond, C. A., Coradini, A., McSween, H. Y., Zuber, M. T., Nathues, A., et al. (2012). Dawn at Vesta: Testing the protoplanetary paradigm. *Science*, *336*(6082), 684–686. https://doi.org/10.1126/science.1219381

Schade, U., & Wäsch, R. (1999). NIR reflectance spectroscopy of mafic minerals in the temperature range between 80 and 473 K. *Advances in Space Research*, *23*(7), 1253–1256. https://doi.org/10.1016/S0273-1177(99)00193-3

Schade, U., Wäsch, R., & Moroz, L. (2004). Near-infrared reflectance spectroscopy of Ca-rich clinopyroxenes and prospects for remote spectral characterization of planetary surfaces. *Icarus*, *168*(1), 80–92. https://doi.org/10.1016/j.icarus.2003.10.016

Scott, E. R. D., Greenwood, R. C., Franchi, I. A., & Sanders, I. S. (2009). Oxygen isotopic constraints on the origin and parent bodies of eucrites, diogenites, and howardites. *Geochimica et Cosmochimica Acta*, *73*(19), 5835–5853. https://doi.org/10.1016/j.gca.2009.06.024

Singer, R. B., & Roush, T. L. (1985). Effects of temperature on remotely sensed mineral absorption features. *Journal of Geophysical Research*, *90*(B14), 12,434–12,444. https://doi.org/10.1029/JB090iB14p12434

Stolper, E. (1975). Petrogenesis of eucrite, howardite, and diogenite meteorites. *Nature*, *258*(5532), 220–222. https://doi.org/10.1038/258220a0

Sunshine, J. M., Bus, S. J., Corrigan, C. M., McCoy, T. J., & Burbine, T. H. (2007). Olivine-dominated asteroids and meteorites: Distinguishing nebular and igneous histories. *Meteoritics & Planetary Science*, *42*(2), 155–170. https://doi.org/10.1111/j.1945-5100.2007.tb00224.x

Thirumalai, K., Singh, A., & Ramesh, R. (2011). A MATLAB code to perform weighted linear regression with (correlated or uncorrelated) errors in bivariate data. *Journal of the Geological Society of India*, *77*(4), 377–380. https://doi.org/10.1007/s12594-011-0044-1

Trang, D., Lucey, P. G., Gillis-Davis, J. J., Cahill, J. T. S., Klima, R. L., & Isaacson, P. J. (2013). Near-infrared optical constants of naturally occurring olivine and synthetic pyroxene as a function of mineral composition. *Journal of Geophysical Research: Planets*, *118*, 708–732. https://doi.org/10.1002/jgre.20072

Trilling, D. E. (2018). SpitzerNEOs results. Retrieved from http://134.114.60.62/db/spitzerneos/results

Turnock, A. C., Lindsley, D. H., & Grover, J. E. (1973). Synthesis and unit cell parameters of Ca-Mg-Fe pyroxenes. *American Mineralogist*, *58*, 50–59.

Warren, P. H., & Jerde, E. A. (1987). Composition and origin of Nuevo Laredo Trend eucrites. *Geochimica et Cosmochimica Acta*, *51*(3), 713–725. https://doi.org/10.1016/0016-7037(87)90082-2